

An Observed Lack of Substructure in Starless Cores II: Super-Jeans Cores

Scott Schnee¹, Sarah Sadavoy^{2,3}, James Di Francesco^{2,3}, Doug Johnstone^{2,3}, Lisa Wei^{4,5}

sschnee@nrao.edu

ABSTRACT

We present SMA and CARMA continuum and spectral line observations of five dense cores located in the Perseus and Ophiuchus molecular clouds whose masses exceed their thermal Jeans masses. Three of these cores have previously been identified as being starless and two have been classified as being possibly protostellar. We find that one core is certainly protostellar. The other four cores, however, are starless and undetected in both C¹⁸O and 1.3 mm continuum emission. These four starless cores have flat density profiles out to at least ~ 0.006 pc, which is typical for starless cores in general. Density profiles predicted by some collapse models, especially in the early stages of infall, are consistent with our observations. Archival data reveal that these starless cores have significant non-thermal support against collapse, although they may still be unstable.

Subject headings: stars: formation; stars: protostars; ISM: jets and outflows

1. Introduction

Recent interferometric observations of supposedly “starless” cores in nearby molecular clouds have found several hidden protostars (e.g., Pineda et al. 2011; Dunham et al. 2011; Schnee et al. 2012; Chen et al. 2012). These observations, however, almost never reveal substructures or evidence for fragmentation in starless cores (Olmí et al. 2005; Schnee et al.

¹National Radio Astronomy Observatory, 520 Edgemont Road, Charlottesville, VA 22903, USA

²National Research Council Canada, Herzberg Institute of Astrophysics, 5071 West Saanich Road Victoria, BC V9E 2E7, Canada

³Department of Physics & Astronomy, University of Victoria, Victoria, BC, V8P 1A1, Canada

⁴Harvard-Smithsonian Center for Astrophysics, 60 Garden Street, Cambridge, MA 02138, USA

⁵Atmospheric and Environmental Research, 131 Hartwell Avenue, Lexington, MA 02421, USA

2010), with some notable exceptions, such as R CrA SMM 1A (Chen & Arce 2010) and L183 (Kirk et al. 2009). The lack of observed substructure in starless cores may imply that stellar multiplicity begins during the protostellar stage. For instance, in the disk fragmentation theory of multiple star formation, a massive accretion disk around a protostar can become unstable and fragment, creating a binary or higher-order system (Adams et al. 1989; Bonnell & Bate 1994). Alternatively, turbulence in starless cores may be forming the seeds of multiplicity (Fisher 2004; Goodwin et al. 2004, 2007), but these seeds may be below the threshold of detectability, as recently suggested by Offner et al. (2012).

In this paper, we present interferometric observations of five cores whose masses derived from dust emission at $850\ \mu\text{m}$ exceed their respective thermal Jeans masses by at least a factor of 2. As such, they are likely to be in the process of forming protostars and/or fragmenting. These cores, given the label “super-Jeans”, were identified by Sadavoy et al. (2010b) and thus make promising targets in the search for substructure in starless cores.

2. Observations

2.1. Previous Observations and Sample Definition

The cores in this study were previously observed at $850\ \mu\text{m}$ with the Submillimeter Common-User Bolometer Array (SCUBA) on the James Clerk Maxwell Telescope (JCMT) (Di Francesco et al. 2008) and at mid- to far-infrared wavelengths with the *Spitzer Space Telescope* (Evans et al. 2003, 2009). Core properties such as mass and size were derived from the SCUBA maps by Sadavoy et al. (2010a), and the classification of each core (i.e., starless, protostellar, or “undetermined”) was made from 3.6-70 μm *Spitzer* maps (Sadavoy et al. 2010b). Sadavoy et al. (2010b) estimated the stability of cores by comparing the Jeans mass for a thermally supported sphere against the core mass derived from dust emission. The Jeans mass is given by

$$M_J = 1.9 \left(\frac{T_d}{10\ \text{K}} \right) \left(\frac{R_J}{0.07\ \text{pc}} \right) M_\odot \quad (1)$$

while the dust-derived mass is given by

$$M = 0.074 \left(\frac{S_{850}}{\text{Jy}} \right) \left(\frac{d}{100\ \text{pc}} \right)^2 \left(\frac{\kappa_{850}}{0.01\ \text{cm}^2\ \text{g}^{-1}} \right)^{-1} \times \left[\exp \left(\frac{17\ \text{K}}{T_d} \right) - 1 \right] M_\odot \quad (2)$$

The dust temperatures (T_d) assumed by Sadavoy et al. (2010b) are 15 K in Ophiuchus and 11 K in Perseus, based on NH_3 surveys of these clouds by Friesen et al. (2009) and Rosolowsky et al. (2008), respectively. The Jeans radius (R_J) and $850\ \mu\text{m}$ flux (S_{850}) are

estimated from the SCUBA observations, the distances assumed are shown in Table 1, and the dust opacity at $850\ \mu\text{m}$ was assumed to be $0.01\ \text{cm}^2\ \text{g}^{-1}$ by Sadavoy et al. (2010b).

Using the data and equations above, Sadavoy et al. (2010b) identified 17 candidate starless cores in nearby molecular clouds whose dust-derived masses exceeded their respective Jeans masses by more than a factor of 2. Based on a simple Jeans analysis, such cores would be expected either to have significant non-thermal support or else to be collapsing and possibly fragmenting. Of these 17 super-Jeans cores, we chose 5 for follow-up observations with the Submillimeter Array (SMA). We chose to observe all 3 of the super-Jeans cores that retained their “starless” classification (Oph-2, Per-2, and Per-6) and 2 of the super-Jeans cores reclassified as “undetermined” (Oph-1 and Per-8) by Sadavoy et al. (2010b). Per-2 and Per-8 were also observed with CARMA. Basic information on these 5 cores is shown in Table 1, and more information about these cores and their properties were described by Sadavoy et al. (2010a,b).

2.2. SMA Calibration

Spectral line observations were taken with the eight-element Submillimeter Array (SMA) (Ho et al. 2004) in June 2010 and October 2010 in the compact-north and compact configurations, respectively. Baselines range from 16 m to 77 m for both configurations, providing sensitivity to spatial scales up to $\sim 8''$ and a resolution of $\sim 3''$ FWHM. The sources were grouped together by RA and observed together in single tracks (Oph-1 and Oph-2 in June; Per-2, Per-6, and Per-8 in October) each about 10 hours in length (see Table 2 for details). The half-power beam width of the 6 m antennas is $54''$ at 230 GHz, and all sources were observed with single pointings.

The receivers were tuned to a rest frequency of 230.538 GHz, Doppler tracked to a recessional velocity (V_{LSR} of $3.95\ \text{km s}^{-1}$ and $7.8\ \text{km s}^{-1}$ for the June and October observations, respectively). The correlator was configured to observe the 1.3 mm continuum with 72 windows, each 104 MHz wide, with a total band width of 7 GHz in the upper and lower sidebands. We also configured four additional windows to observe the $^{12}\text{CO}(2-1)$ and $^{13}\text{CO}(2-1)$ lines with 406 kHz ($0.5\ \text{km s}^{-1}$) resolution, the C^{18}O line with 203 kHz ($0.25\ \text{km s}^{-1}$) resolution, and the $\text{N}_2\text{D}^+(3-2)$ line with 813 kHz ($1\ \text{km s}^{-1}$) resolution (see Table 3). The $^{13}\text{CO}(2-1)$ and $\text{N}_2\text{D}^+(3-2)$ lines were only marginally detected towards one core (Per-8), so neither transition is discussed further in this paper. $\text{C}^{18}\text{O}(2-1)$ was detected only towards Per-8.

The data were reduced using the MIR package. We flagged the data for bad channels, antennas, weather, and pointing. Radio pointing was done at one hour after sunset for

each track. We calibrated the bandpass with a bright quasar, 3C 454.3, for both tracks. Atmospheric calibration was done with observations of the quasars 1625-254 and 1517-243 in the June track and 0036+323 and 0319-415 in the October track every 15 minutes. Absolute flux calibration was done using observations of Uranus.

2.3. CARMA Calibration

Spectral line observations in the 1 mm window were obtained with CARMA, a 15-element interferometer consisting of nine 6.1-meter antennas and six 10.4-meter antennas. The CARMA observations were taken in D-array for both observations, with baselines ranging from 11 m to 150 m, providing sensitivity to spatial scales up to $\sim 12''$ and a resolution of $\sim 2''$ FWHM. The sources Per-2 and Per-8 were observed in single pointings in separate tracks in May 2011 and June 2011, respectively, each for about 4.5 hours (see Table 2 for details).

The receivers were tuned to a rest frequency of 230.538 GHz and Doppler tracked to a recessional velocity (V_{LSR}) of 7.8 km s^{-1} . The correlator was configured to observe the 1.3 mm continuum with 7 bands, each with an upper and lower sideband, with 495 MHz band width with 39 channels per band, providing a total band width of 7 GHz. One band was configured to observe C^{17}O (2-1) in the lower sideband and CO (2-1) in the upper sideband, each with 781 kHz spectral resolution ($\sim 1 \text{ km s}^{-1}$) and 123 MHz band width (See Table 3).

The data were reduced using the MIRIAD package (Sault et al. 1995). We flagged the data for bad channels, antennas, weather, and pointing. Radio pointing was done at the beginning of each track and pointing constants were updated at least every two hours thereafter, using either radio or optical pointing routines (Corder et al. 2010). We calibrated the bandpass and gains using observations of the bright quasar 3C84, which was observed for 3 minutes out of each 21 minute source-calibrator cycle. Absolute flux calibration was done using observations of Mars and the consistency of flux measurements with the SMA data set.

Due to instrumental problems, the upper sideband of the spectral line band was lost, so our observations of CO (2-1) come from the SMA only. C^{17}O (2-1) was detected only towards Per-8.

2.4. Imaging

We imaged the SMA and CARMA continuum and line emission from each source using MIRIAD (Sault et al. 1995), with natural weighting and an additional weighting in inverse proportion to the noise as estimated by the system temperature. Each data cube was cleaned to a cutoff of 2σ in the residual image. The 1.3 mm continuum data for the source Per-8 came from both CARMA and the SMA, while all other maps have data from only one array. The combined CARMA+SMA 1.3 mm continuum map of Per-8 has an rms of 6 mJy beam^{-1} and a beam size of $2.7'' \times 2.0''$.

3. Analysis

3.1. Per-8

Continuum emission at 1.3 mm is detected from Per-8, with a peak flux of $380 \text{ mJy beam}^{-1}$ and an integrated flux of 750 mJy . The peak of the dust emission seen with SMA and CARMA is at (J2000) 3:32:17.923 +30:49:47.869, and this is also the peak of the detected C^{17}O (2-1) and C^{18}O (2-1) integrated intensity.

Sadavoy et al. (2010a) initially classified Per-8 as “starless,” after rejecting a nearby compact source of mid-infrared emission detected by *Spitzer* in the IRAC and MIPS bands (SSTc2dJ033218.0+304947) as non-protostellar. This compact source has colors similar to those of star-forming galaxies (e.g., using the prescription from Gutermuth et al. 2008) rather than the colors expected for embedded protostars (e.g., following Evans et al. 2009). Since such color analyses are not perfect and may throw out legitimate protostellar sources, Sadavoy et al. (2010b) reclassified Per-8 as “undetermined.” Indeed, Per-8 was classified as a Class 0 protostar by Hatchell & Dunham (2009), who identified an outflow from the core. Near-infrared maps of the Perseus B1 region also show shocked emission from an outflow driven by Per-8 (Walawender et al. 2009).

Given the previous observations of this source, it is not surprising that we detect a collimated $\text{CO}(2-1)$ outflow from Per-8. The outflow is centered on the 1.3 mm continuum source, which is also coincident with the compact source detected with *Spitzer*. In Figure 1, we show the outflow, the 1.3 mm continuum, and a C^{18}O (2-1) velocity map with the possible signature of a rotating disk. For the analysis of Per-8, fits to the observed spectra were made only for those profiles that had three independent velocity channels with a signal-to-noise ratio greater than 5. In Figure 2, example spectra of C^{18}O (2-1) and C^{17}O (2-1) at the peak of the line emission are shown. In Figure 3, we show that the 1.3 mm continuum emission

presented here is spatially coincident with the IRAC source noted by Sadavoy et al. (2010b) and the peak of the SCUBA 850 μm emission.

Per-8 shows that some cores cannot be accurately classified solely from infrared continuum maps and assumed protostellar colors. For example, strong PAH emission or shocks from outflows may cause excess emission in some of the IRAC bands and skew the infrared colors (e.g., Gutermuth et al. 2008). Assumed protostellar colors are determined based on a best-effort basis, and only select objects *most likely* to be protostars. Furthermore, the photometry of Per-8 is complicated by it being a resolved source and by its location on the boundary between two c2d mosaic tiles. Occasionally misclassified cores like Per-8 should be expected and caution is necessary when using only infrared continuum maps to determine if cores are starless or protostellar.

3.2. Oph-1, Oph-2, Per-2, and Per-6

The 1.3 mm continuum emission from the remaining 4 cores in this survey is not detected by our SMA and CARMA observations. We calculate upper limits to the masses of point sources that could have been detected in these observations from the respective rms values reported in Table 2 and using Equation 2 scaled to 1.3 mm with an assumed emissivity spectral index of $\beta = 2$. The 3σ upper limits on the mass of a point source embedded in Oph-1, Oph-2, Per-2, and Per-6 are $0.002 M_{\odot}$, $0.002 M_{\odot}$, $0.01 M_{\odot}$, and $0.02 M_{\odot}$ respectively. Had we assumed a lower dust temperature of 5.5 K, as reported by Crapsi et al. (2007) at the center of L1544, our reported mass upper limits would be increased by a factor of 4-5. In comparison, the median 3σ upper limit of the mass of compact structures in starless cores in Perseus reported by Schnee et al. (2010) is $0.2 M_{\odot}$, so this survey goes a factor of 10-100 deeper than Schnee et al. (2010). The improved mass sensitivity in this paper is primarily a result of the wavelengths of observations (1.3 mm here vs. 3 mm by Schnee et al. 2010) and the λ^{-4} dependence of the dust emission. We conclude that Oph-1, Oph-2, Per-2, and Per-6 are true starless cores, based on the non-detection of compact continuum down to a few Jupiter masses. In addition to being undetected in the 1.3 mm continuum maps, Oph-1, Oph-2, Per-2, and Per-6 show no signs of outflows in the CO and ^{13}CO maps. The non-detection of outflows from these cores further suggests that they are indeed starless. Furthermore, these four cores are not detected in the N_2D^+ , C^{18}O , or C^{17}O line maps made with the SMA and CARMA.

3.2.1. Density Profiles

To analyze further the meaning of non-detections of continuum emission from starless cores, we simulate observations of the 1.3 mm dust emission from idealized cores. We assumed a typical density distribution (Tafalla et al. 2004) of

$$n = \frac{n_0}{1 + \left(\frac{r}{r_0}\right)^{2.5}} \quad (3)$$

where n_0 is normalized such that the total core mass within a radius of 0.05 pc is $5 M_\odot$. This density profile has a flat interior (at radii less than r_0) and a steep exterior (at radii greater than r_0). The radius r_0 varies from 0.002 pc to 0.02 pc in our simulations, as shown in Figure 4. We used an outer radius of 0.05 pc, as is typical of starless cores. We assumed a dust emissivity at 1.3 mm of $0.009 \text{ cm}^2 \text{ g}^{-1}$, as given in Table 1, column 5 of Ossenkopf & Henning (1994) for dust grains with thin ice mantles at a density of 10^6 cm^{-3} . We assumed a distance to the cores of 250 pc, appropriate for cores in the Perseus molecular cloud (Hirota et al. 2008; Lombardi et al. 2010). In one set of simulations, we assumed an isothermal dust temperature of 10 K, appropriate for starless cores in Perseus (Schnee et al. 2009). In a second set of simulations, we assumed the dust temperature profile derived for the starless core L1544 by Crapsi et al. (2007).

$$T(r) = T_{out} - \frac{T_{out} - T_{in}}{1 + (r/r_{0,T})^{1.5}} \quad (4)$$

where T_{out} is the temperature in the outer layer of the core and had a value of 12 K, T_{in} is the temperature at the center of the core and had a value of 5.5 K, and $r_{0,T}$ had a value of 0.012 pc.

The 2-dimensional flux distribution was predicted for each core, and this was used as input for the simulated observations with SMA. We used the Common Astronomy Software Applications (CASA)¹ software package to simulate a 5-hour track on each core, centered on transit, with thermal noise equal to $0.5 \text{ mJy beam}^{-1}$, which is similar to the observations described in Section 2.2.

As shown in Figure 4, simulated isothermal cores with more compact density distributions ($r_0 \leq 0.009 \text{ pc}$) would have been detected with 5σ confidence, while cores with larger central flat regions ($r_0 > 0.009 \text{ pc}$) are resolved out by the simulated SMA observations. To be consistent with the observations presented here, cores with a more realistic temperature

¹<http://casa.nrao.edu>

profile and small central flat density profile ($r_0 \leq 0.006$ pc) are ruled out, as shown in Figure 5.

Since we do not detect any of the starless cores in our sample, we estimate that their density profiles are flat on scales out to at least 0.01 pc, assuming isothermality. Allowing for an expected temperature drop toward the core center, we find that these cores must be flat out to scales larger than 0.006 pc. The density profiles that we find are in excellent agreement with previous single-dish observations. For example, Ward-Thompson et al. (1999) mapped with the IRAM 30 m telescope the 1.3 mm continuum emission from a sample of nearby starless cores and found that their flux distributions were flat out to 0.01-0.02 pc. The smoothness of the continuum emission from starless cores found in this study is also in agreement with the results of Schnee et al. (2010) and Offner et al. (2012).

3.2.2. Collapse Rate

Based on a simple Jeans analysis, these starless cores may be unstable and therefore in the process of collapsing. The non-detection of continuum emission from the starless cores in our sample, however, is inconsistent with collapse models that predict strongly peaked density distributions, such as those seen in expansion wave models (Silk & Suto 1988). The early stages of slow contraction, such as in models of ambipolar diffusion (e.g., Safier et al. 1997) and models of the pressure-free collapse of Bonnor-Ebert spheres (e.g., Myers 2005), have flat density distributions at small radii and are consistent with our observations. Similarly, the initial stages of uniform collapse (Silk & Suto 1988) are also consistent with our observations. The infall rate, in a freefall approximation, for a $5 M_{\odot}$ object to collapse from an initial radius of 0.1 pc to 0.05 pc (roughly the radius of the cores in this sample) is approximately 0.2 km s^{-1} . Collapse at this rate can be easily detected in starless cores, as the typical line width is comparable to this infall speed (Foster et al. 2009). We suggest that super-Jeans starless cores are good targets for future observations to look for infall.

3.2.3. Stability Against Collapse

The reported values of M/M_J for Oph-1, Oph-2, Per-2 and Per-6 are 2.2, 2.3, 4.8 and 4.9 (Sadavoy et al. 2010b) respectively, for a Jeans mass derived from thermal support only. Although the starless cores in this paper are super-Jeans when considering only thermal support, we can estimate their stability when also accounting for their non-thermal motions. For this analysis, we looked at archival data of the published velocity dispersions for these

cores. Rosolowsky et al. (2008) have published the NH_3 (1,1) velocity dispersions of Per-2 and Per-6, i.e., 0.31 km s^{-1} and 0.46 km s^{-1} respectively. The N_2H^+ (1-0) velocity dispersions of Per-2 and Per-6, 0.33 km s^{-1} and 0.32 km s^{-1} , are similar to the ammonia line dispersions (Johnstone et al. 2010). The typical velocity dispersion measured in NH_3 spectra of starless cores in Perseus is $<0.2 \text{ km s}^{-1}$ (Foster et al. 2009), so Per-2 and Per-6 have especially large non-thermal motions. The velocity dispersion due to thermal motions NH_3 at 10 K is $\sim 0.07 \text{ km s}^{-1}$, or about $4\text{-}6\times$ smaller than the observed dispersions measured from ammonia spectra of Per-2 and Per-6. Friesen et al. (2009) and Roueff et al. (2005) have published the NH_3 and ND_3 velocity dispersions for regions near Oph-1 and Oph-2, which have values of 0.16 km s^{-1} and 0.18 km s^{-1} , about 2 times larger than the thermal velocity dispersion.

To determine the stability of the starless cores in our sample, including the non-thermal motions, we calculate a “typical” virial mass for a uniform density core, following Bertoldi & McKee (1992).

$$M_{\text{vir}} = \frac{5R\sigma^2}{G} \quad (5)$$

Taking values typical of the starless cores in this sample ($\sigma = 0.4 \text{ km s}^{-1}$ and $R = 0.05 \text{ pc}$), we find that a typical virial mass is $\sim 9 M_{\odot}$ (or roughly $4.5 M_{\odot}$ for a density distribution of a critically stable Bonnor-Ebert sphere). Given that the actual masses of the cores are approximately equal to the Bonnor-Ebert virial mass, we can not be completely confident that the cores are bound or gravitationally unstable. The uncertainties in the true core masses and non-thermal support, however, are significant. Indeed, the large line widths seen in these cores could be interpreted as coming from a structured velocity field (from infall itself, for example), and may not be an indication of turbulent support at all. We note also that the manner in which the observed non-thermal motions might supply pressure support without significant dissipation is still unclear. High angular resolution observations of the velocity fields around these cores can distinguish between these possibilities.

4. Summary

In this paper, we presented new SMA and CARMA observations of five super-Jeans cores that have been previously classified as being candidate “starless” or “undetermined” by Sadavoy et al. (2010b). We find, in agreement with previous observations, that the core Per-8 is actually protostellar and is the origin of a collimated bipolar outflow. The cores Oph-1, Oph-2, Per-2, and Per-6 are truly starless, however, with non-detections in the 1.3 mm continuum corresponding to 3σ upper limits to the mass of any embedded point source of

$\leq 0.02 M_{\odot}$. Our simulations suggest that these four cores have flat density profiles out to radii of at least ~ 0.006 – 0.01 pc, in agreement with previous single-dish and interferometric observations of starless cores. Although Oph-1, Oph2, Per-2, and Per-6 are super-Jeans when considering only their thermal support, when non-thermal support is considered their stability against collapse is much more uncertain.

We thank Robert Gutermuth for helpful discussion on the nature of Per-8. We thank our anonymous referee for suggestions that improved this paper. The National Radio Astronomy Observatory is a facility of the National Science Foundation operated under cooperative agreement by Associated Universities, Inc. JDF acknowledges support by the National Research Council of Canada and the Natural Sciences and Engineering Council of Canada (via a Discovery Grant). DJ is supported by a Natural Sciences and Engineering Research Council of Canada (NSERC) Discovery Grant. The Submillimeter Array is a joint project between the Smithsonian Astrophysical Observatory and the Academia Sinica Institute of Astronomy and Astrophysics and is funded by the Smithsonian Institution and the Academia Sinica. Support for CARMA construction was derived from the Gordon and Betty Moore Foundation, the Kenneth T. and Eileen L. Norris Foundation, the James S. McDonnell Foundation, the Associates of the California Institute of Technology, the University of Chicago, the states of California, Illinois, and Maryland, and the National Science Foundation. Ongoing CARMA development and operations are supported by the National Science Foundation under a cooperative agreement, and by the CARMA partner universities.

Facilities: SMA, CARMA

REFERENCES

- Adams, F. C., Ruden, S. P., & Shu, F. H. 1989, *ApJ*, 347, 959
- Bertoldi, F., & McKee, C. F. 1992, *ApJ*, 395, 140
- Bonnell, I. A., & Bate, M. R. 1994, *MNRAS*, 269, L45
- Chen, X., & Arce, H. G. 2010, *ApJ*, 720, L169
- Chen, X., Arce, H. G., Dunham, M. M., et al. 2012, arXiv:1203.5252
- Corder, S. A., Wright, M. C. H., & Carpenter, J. M. 2010, *Proc. SPIE*, 7733,
- Crapsi, A., Caselli, P., Walmsley, M. C., & Tafalla, M. 2007, *A&A*, 470, 221

- Di Francesco, J., Johnstone, D., Kirk, H., MacKenzie, T., & Ledwosinska, E. 2008, *ApJS*, 175, 277
- Dunham, M. M., Chen, X., Arce, H. G., et al. 2011, *ApJ*, 742, 1
- Enoch, M. L., Lee, J.-E., Harvey, P., Dunham, M. M., & Schnee, S. 2010, *ApJ*, 722, L33
- Evans, N. J., II, Allen, L. E., Blake, G. A., et al. 2003, *PASP*, 115, 965
- Evans, N. J., II, Dunham, M. M., Jørgensen, J. K., et al. 2009, *ApJS*, 181, 321
- Fisher, R. T. 2004, *ApJ*, 600, 769
- Foster, J. B., Rosolowsky, E. W., Kauffmann, J., et al. 2009, *ApJ*, 696, 298
- Friesen, R. K., Di Francesco, J., Shirley, Y. L., & Myers, P. C. 2009, *ApJ*, 697, 1457
- Goodwin, S. P., Whitworth, A. P., & Ward-Thompson, D. 2004, *A&A*, 414, 633
- Goodwin, S. P., Kroupa, P., Goodman, A., & Burkert, A. 2007, *Protostars and Planets V*, 133
- Gutermuth, R. A., Bourke, T. L., Allen, L. E., et al. 2008, *ApJ*, 673, L151
- Hatchell, J., & Dunham, M. M. 2009, *A&A*, 502, 139
- Hirota, T., Bushimata, T., Choi, Y. K., et al. 2008, *PASJ*, 60, 37
- Ho, P. T. P., Moran, J. M., & Lo, K. Y. 2004, *ApJ*, 616, L1
- Johnstone, D., Rosolowsky, E., Tafalla, M., & Kirk, H. 2010, *ApJ*, 711, 655
- Kirk, J. M., Crutcher, R. M., & Ward-Thompson, D. 2009, *ApJ*, 701, 1044
- Ladd, E. F., Fuller, G. A., & Deane, J. R. 1998, *ApJ*, 495, 871
- Lombardi, M., Lada, C. J., & Alves, J. 2010, *A&A*, 512, A67
- Myers, P. C. 2005, *ApJ*, 623, 280
- Offner, S. S. R., Capodilupo, J., Schnee, S., & Goodman, A. A. 2012, *MNRAS*, 420, L53
- Olmi, L., Testi, L., & Sargent, A. I. 2005, *A&A*, 431, 253
- Ossenkopf, V., & Henning, T. 1994, *A&A*, 291, 943
- Pineda, J. E., Arce, H. G., Schnee, S., et al. 2011, *ApJ*, 743, 201

- Rosolowsky, E. W., Pineda, J. E., Foster, J. B., et al. 2008, ApJS, 175, 509
- Roueff, E., Lis, D. C., van der Tak, F. F. S., Gerin, M., & Goldsmith, P. F. 2005, A&A, 438, 585
- Sadavoy, S. I., Di Francesco, J., & Johnstone, D. 2010b, ApJ, 718, L32
- Sadavoy, S. I., Di Francesco, J., Bontemps, S., et al. 2010a, ApJ, 710, 1247
- Safier, P. N., McKee, C. F., & Stahler, S. W. 1997, ApJ, 485, 660
- Sault, R. J., Teuben, P. J., & Wright, M. C. H. 1995, Astronomical Data Analysis Software and Systems IV, 77, 433
- Schnee, S., Rosolowsky, E., Foster, J., Enoch, M., & Sargent, A. 2009, ApJ, 691, 1754
- Schnee, S., Enoch, M., Johnstone, D., et al. 2010, ApJ, 718, 306
- Schnee, S., Di Francesco, J., Enoch, M., et al. 2012, ApJ, 745, 18
- Silk, J., & Suto, Y. 1988, ApJ, 335, 295
- Tafalla, M., Myers, P. C., Caselli, P., & Walmsley, C. M. 2004, A&A, 416, 191
- Walawender, J., Reipurth, B., & Bally, J. 2009, AJ, 137, 3254
- Ward-Thompson, D., Motte, F., & Andre, P. 1999, MNRAS, 305, 143

This preprint was prepared with the AAS L^AT_EX macros v5.2.

Table 1. Summary of Dense Core Properties

Name ¹	Nearby Sources ¹	RA J2000	Dec J2000	Molecular Cloud	Distance pc	Mass ¹ M _⊙	R _{eff} ¹ pc
Oph-1	...	16:26:59.20	-24:34:20.0	Ophiuchus	125	5.3	0.060
Oph-2	IRAS 16293-2422E	16:32:29.00	-24:29:06.0	Ophiuchus	125	3.2	0.038
Per-2	...	03:28:59.50	+31:21:31.0	Perseus	250	7.6	0.053
Per-6	...	03:29:08.70	+31:15:13.0	Perseus	250	8.1	0.055
Per-8	IRAS 03292-3039	03:32:17.60	+30:49:47.0	Perseus	250	7.2	0.055

¹From Sadavoy et al. (2010b)

Table 2. SMA and CARMA Map Properties

Name	Beam size ¹ "	Continuum rms ^{1,2} mJy beam ⁻¹	C ¹⁸ O rms ^{1,3} mJy beam ⁻¹	Beam size ⁴ "	Continuum rms ^{4,2} mJy beam ⁻¹	C ¹⁷ O rms ^{4,5} mJy beam ⁻¹
Oph-1	3.3 × 2.4	0.54	150			
Oph-2	3.3 × 2.4	0.63	150			
Per-2	3.7 × 2.4	0.61	120	2.2 × 1.7	2.4	73
Per-6	3.7 × 2.4	0.75	72			
Per-8	3.7 × 2.4	2.5	69	2.2 × 1.8	8.8	79

¹SMA observations

²Over the 7 GHz band width

³Per 0.28 km s⁻¹ channel

⁴CARMA observations

⁵Per 1 km s⁻¹ channel

Table 3. Observations

Observatory	Continuum/Line	ν^1 GHz	Channel Spacing kHz	Band width MHz
SMA	1.3 mm continuum	224.538	812	7000
SMA	CO (2-1)	230.538	406	104
SMA	¹³ CO (2-1)	220.399	406	104
SMA	C ¹⁸ O (2-1)	219.560	203	104
SMA	N ₂ D ⁺ (3-2)	231.322	812	104
CARMA	1.3 mm continuum	227.638	812	7000
CARMA	CO (2-1)	230.538	781	124
CARMA	C ¹⁷ O (2-1)	224.714	781	124

¹Rest frequency

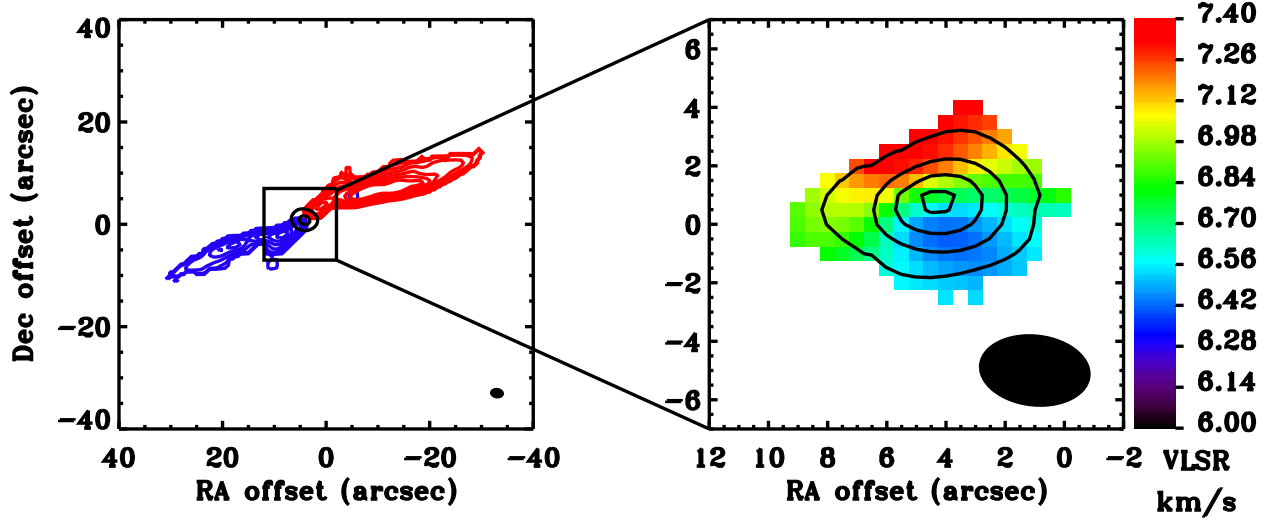


Fig. 1.— Interferometer data of Per-8. (*left*) Black contours show the 1.3 mm continuum emission from Per-8, at values of 0.1 Jy beam^{-1} and 0.3 Jy beam^{-1} . Red and blue contours show the redshifted and blueshifted CO (2–1) integrated intensity, beginning at a value of 3 K km s^{-1} and increasing with steps of 3 K km s^{-1} . Redshifted emission is integrated over LSR velocities between 9 km s^{-1} and 18 km s^{-1} , and blueshifted emission is integrated over LSR velocities between -2 km s^{-1} and 5 km s^{-1} . The synthesized beam of the continuum emission is shown in the bottom right corner of the panel. (*right*) Black contours show the the integrated intensity of the C^{18}O (2–1) emission beginning at a value of 2 K km s^{-1} and increasing with steps of 2 K km s^{-1} . Color shows the centroid velocity from Gaussian fits to the C^{18}O (2–1) spectra. The synthesized beam of the C^{18}O (2–1) data is shown in the bottom right corner of the panel. Note that the synthesized beams of continuum ($2.7'' \times 2.0''$) and CO ($3.7'' \times 2.4''$) data differ because the former come from CARMA and the SMA, while the latter only come from the SMA.

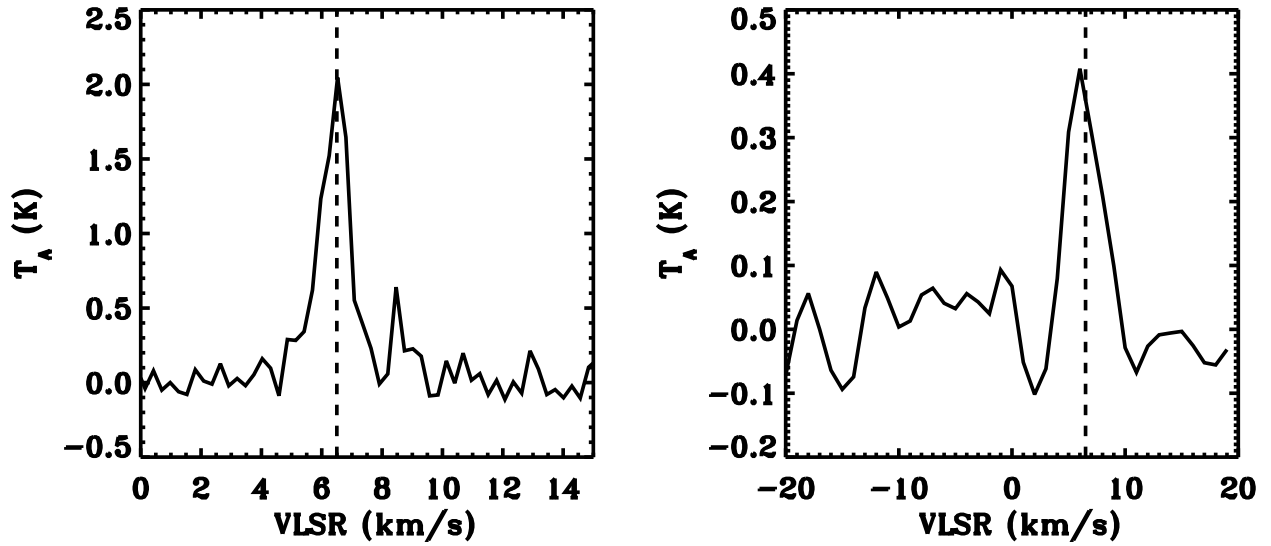


Fig. 2.— Spectra towards Per-8. (*left*) $C^{18}O$ (2-1) spectrum taken at the peak of the $C^{18}O$ (2-1) integrated intensity (J2000 3:32:17.87, +30:49:47). (*right*) $C^{17}O$ (2-1) spectrum taken at the peak of the $C^{17}O$ (2-1) integrated intensity (same location as for $C^{18}O$ (2-1)). The vertical dashed line in both panels shows a velocity of 6.5 km s^{-1} and is plotted to guide the eye and show that the $C^{18}O$ (2-1) and $C^{17}O$ (2-1) spectra peak at the same velocity.

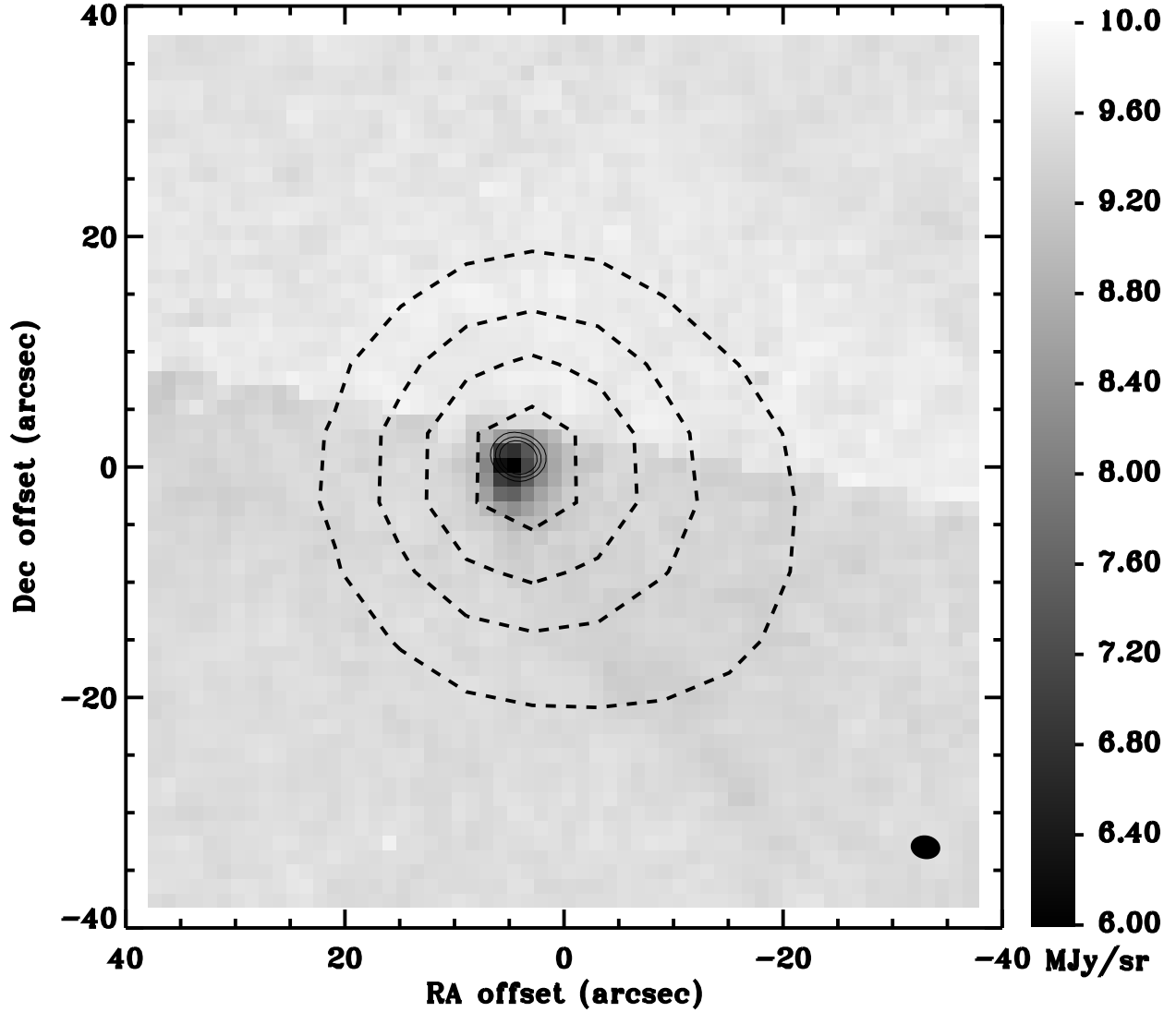


Fig. 3.— Continuum data of Per-8. Greyscale shows the *Spitzer* IRAC Band 4 ($8\ \mu\text{m}$) emission from the region around Per-8. The 1.3 mm continuum emission detected with SMA and CARMA (thin solid contours at 100 mJy/beam, 150 mJy/beam, and 200 mJy/beam) are coincident with the $8\ \mu\text{m}$ emission. The thick dashed contours show the $850\ \mu\text{m}$ emission (at 0.5, 1.0, 1.5, and 2.0 Jy/beam) from Per-8 detected with SCUBA (Di Francesco et al. 2008).

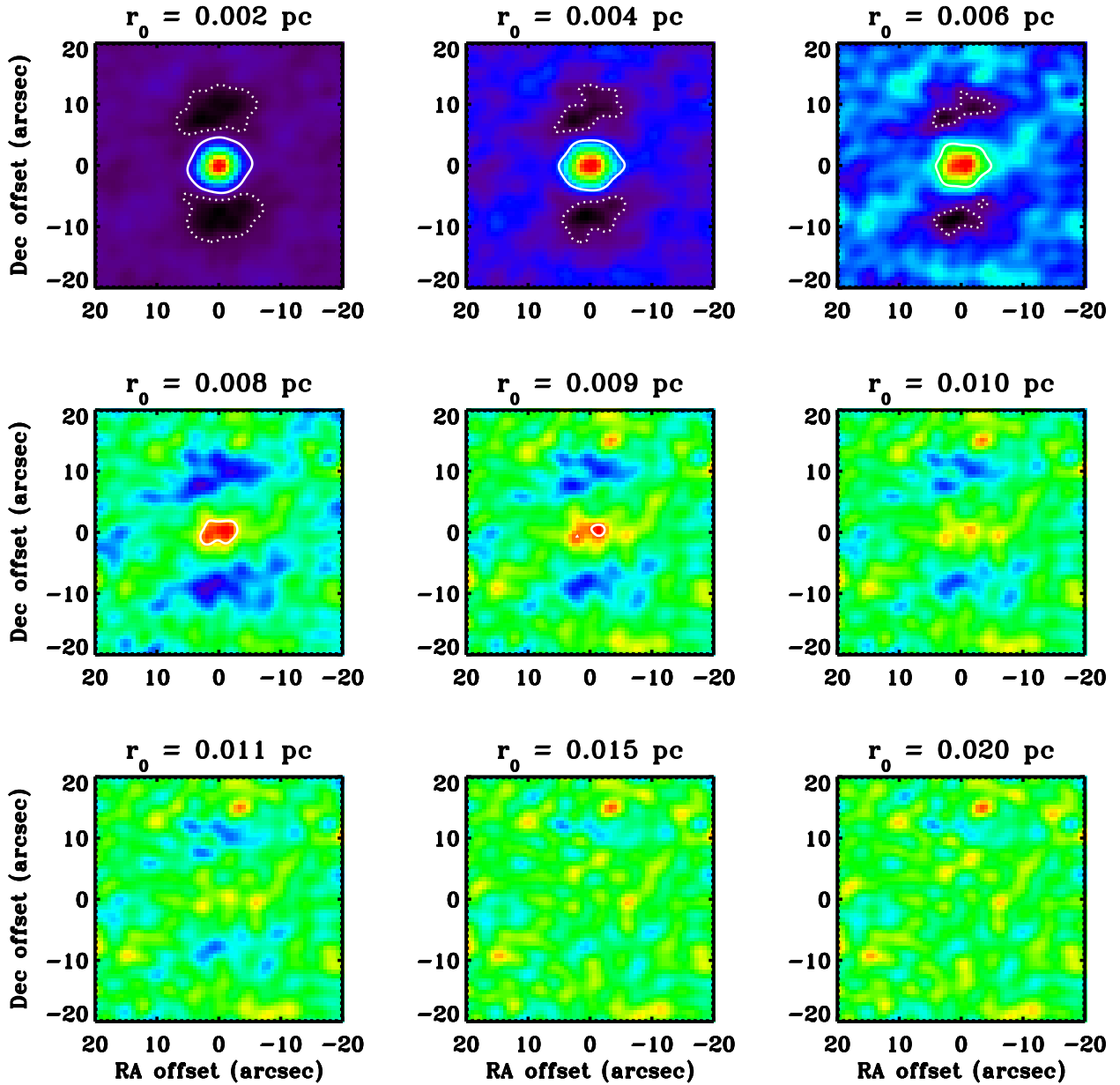


Fig. 4.— Simulated SMA compact array maps of starless cores of constant temperature ($T_d = 10$ K) in the Perseus molecular cloud. The observations are described in Section 3.2. The radius inside of which the density profile is flat is labeled for each panel. The thermal noise in each map is $0.5 \text{ mJy beam}^{-1}$. The solid contours show emission at $2.5 \text{ mJy beam}^{-1}$ and the dashed contours show emission at $-2.5 \text{ mJy beam}^{-1}$. There is no $\pm 5\sigma$ emission for $r_0 \geq 0.01$ pc. Regions of negative flux are artefacts originating from incomplete sampling of the Fourier transform of the sky brightness distribution.

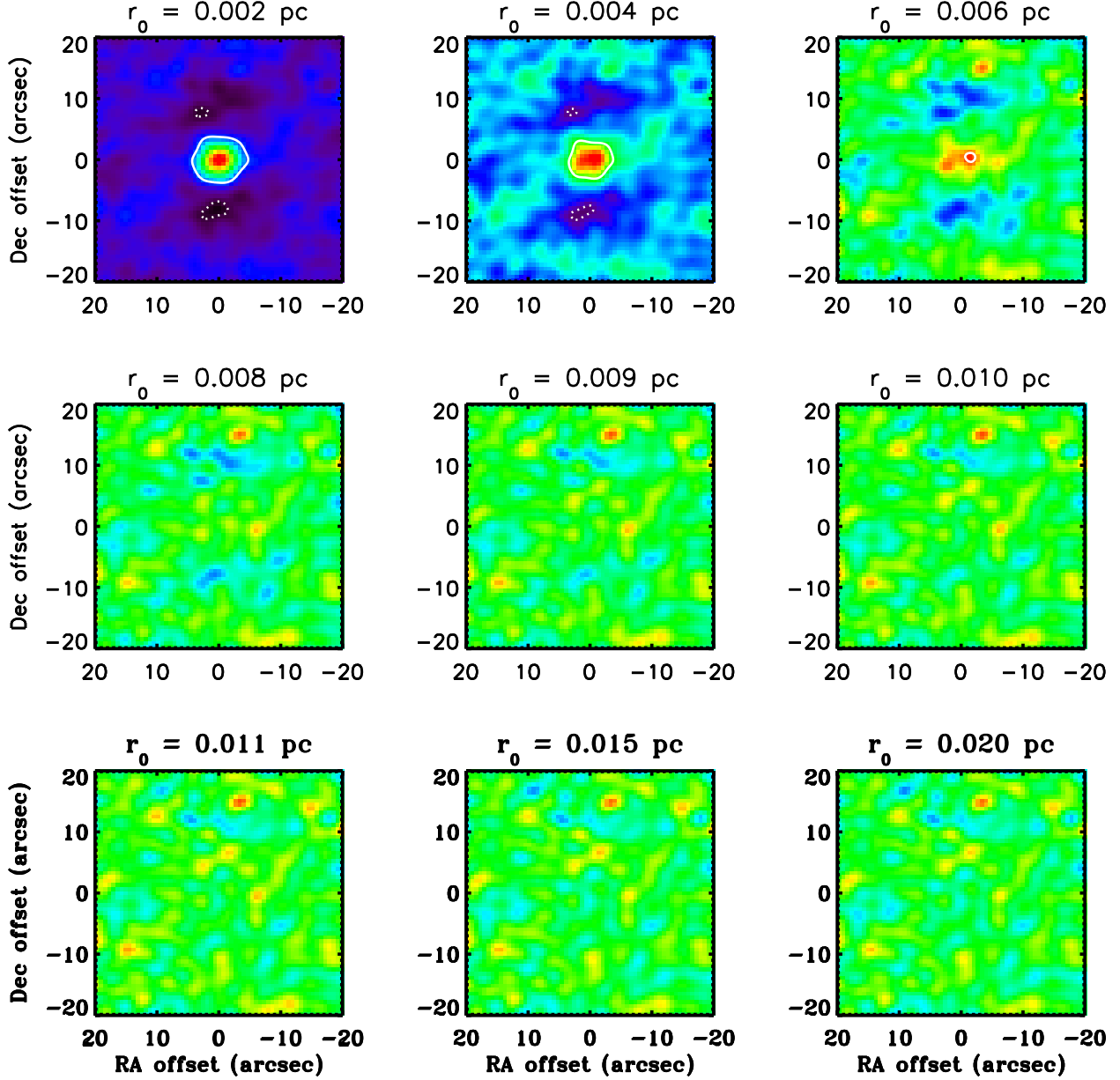


Fig. 5.— Same as Figure 4, but for cores with a temperature profile given by Equation 4. In comparison with Figure 4, the only cores that are detected in these simulations with at least 5σ confidence are those with $r_0 \leq 0.006$ pc. There is no $\pm 5\sigma$ emission for $r_0 \geq 0.008$ pc.